Mössbauer study of the Ising antiferromagnet $DyPO_4$: Hyperfine parameters, g-factor anisotropy, and spin-lattice relaxation

D. W. Forester and W. A. Ferrando*†
Naval Research Laboratory, Washington, D. C. 20375
(Received 24 September 1975)

Mössbauer spectroscopy of the 26-keV γ-ray transition in ^{161}Dy was employed to study nuclear hyperfine interactions in Ising-like $DyPO_4$. Single-crystal and polycrystalline samples were studied over the temperature range $1.8 \leq T \lesssim 300$ K, which included the Néel temperature $T_N = 3.39$ K. For $0 \leq T \lesssim 10$ K the spectra could be analyzed in terms of a "static" $S = \frac{1}{2}$ spin Hamiltonian $\mathcal{H} = A_z I_z S_z + (A_\perp/2)(I^+S^- + I^-S^+) + P[3I_z^2 - I(I+1)]$. The measured components of the magnetic hyperfine tensor parallel and perpendicular to the tetragonal c axis are, respectively, $A_z/2 = -831 \pm 4$ MHz and $A_\perp = -14 \pm 5$ MHz. This is the first reported measurement of an $A_\perp$ term in Mössbauer studies of dysprosium compounds. Using the known ionic g-factor component, $g_z = 19.32 \pm 0.01$, we calculate $k = A_z/2hg_z = 43.0 \pm 0.2$ and hence $g_\perp = 0.3 \pm 0.1$. The ratio of quadrupole parameters for the excited and ground nuclear states of ^{161}Dy is $P_e/P_g = 0.986 \pm 0.003$ with $P_g/h = 60.3 \pm 0.6$ MHz. For $T \gtrsim 10$ K the spectra are relaxation broadened and can be described well using the time-dependent Hamiltonian $\mathcal{H}(t) = f(t)A_z I_z S_z + P[3I_z^2 - I(I+1)]$, where $f(t) = \pm 1$. These spectra were analyzed using a random-fluctuation stochastic model for $f(t)$ and incorporating the exchange splittings obtained from previous optical work on the ground Kramers doublet. The analysis then depends on a single relaxation parameter $\Omega(T)$. Between $T = 16$ and 36 K the relaxation is dominated by an Orbach spin-lattice process of the form $\Omega = \Omega_0 e^{-\Delta_G/T}$, where $\Delta_G \simeq 70$ cm^{-1}.

I. INTRODUCTION

The nuclear hyperfine structure (hfs) spectra of ^{161}Dy were studied in both single-crystal[1] and polycrystalline samples of $DyPO_4$. Measurements were made over the temperature range $1.8 \lesssim T \lesssim 300$ K which includes the Néel temperature $T_N = 3.39$ K.[2]

$DyPO_4$ has the tetragonal zircon ($ZrSiO_4$) type crystal structure[3] as do most of the rare-earth ortho-phosphates, -vanadates, and -arsenates. The space group is D_{4h}^{19}, while the point symmetry about a Dy^{3+} ion is D_{2d}. The crystallographic structure is shown in Fig. 1 and the unit-cell dimensions are $a_0 = 6.917$ Å and $c_0 = 6.053$ Å.[4] Below T_N the magnetic structure[5] can be considered in terms of two interpenetrating body-centered-tetragonal sublattices. Each Dy^{3+} on one sublattice has four nearest neighbors which lie on the other sublattice. No evidence has been found which would indicate a spontaneous low-temperature lattice distortion such as that observed in $DyVO_4$.[6]

Much of the interest in $DyPO_4$ has centered on its nearly Ising magnetic behavior. The results of a variety of experiments including magnetoelectric effect,[7] optical,[8-11] magnetic susceptibility,[2,9] and heat-capacity[2,9] measurements are in excellent agreement with exact theoretical calculations[12] based on a low-temperature series expansion and near-neighbor-only Ising interactions. Optical[8,9] and far-infrared EPR[10,11] studies have shown the lowest Dy^{3+} state to be an exchange plus dipole-split Kramers doublet of almost pure $|J_z = \pm\frac{15}{2}\rangle$ character. The first excited crystal-field state is about 70 cm^{-1} (108 K) above this.[10,11] The crystalline electric field (CEF) produces a highly anisotropic $\tilde{g}$ tensor in the ground doublet which is responsible for the observed Ising behavior. A value of[11] $g_z = 19.32 \pm 0.01$ is measured parallel to the tetragonal c axis whereas $g_\perp$ is quite small. Wright *et al.*[9] first reported a value of $g_\perp = 0.5 \pm 0.5$ with the error due primarily to the extreme sensitivity to misalignment of the crystal in a magnetic field. More recently, a value of[11] $g_\perp = 0.7 \pm 0.1$ was deduced by integrating the intensity of the ground-state magnetic resonance spectrum obtained in an external field large enough to saturate the spin system.

There were a number of reasons for undertaking the present study of $DyPO_4$. The local D_{2d} symmetry of Dy^{3+}, the large separation of the first excited CEF state from the ground Kramers doublet, and the Ising behavior of the spin system all provide simplification for the extraction of static hyperfine interaction parameters and dynamic spin-relaxation parameters from the Mössbauer spectra. A spin Hamiltonian can be used which involves only the nuclear magnetic hyperfine tensor components A_z and $A_\perp$ parallel and perpendicular to the tetragonal c axis and an axial quadrupole parameter P also along the c axis. Because of the Ising nature, relaxation is expected to be domin-

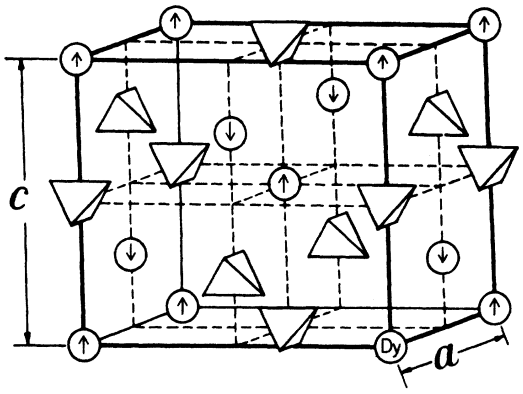

FIG. 1. Unit cell of $DyPO_4$. The Dy^{3+} site symmetry is D_{2d}. The arrows at each Dy^{3+} site indicate the moment directions below $T_N = 3.39$ K.

ated by spin-lattice relaxation. Likewise, the time evolution of the spectra can be calculated assuming modulation of the γ-ray energy produced by random flipping of the ion spin between the two states of the spin $S = \frac{1}{2}$ Hamiltonian. For the first time, one has available the measured exchange splittings of the ground state as a function of temperature.[8,9] These can be folded into the relaxation analysis so that only one independent parameter, the relaxation frequency $\Omega(T)$, remains. The lack of precise knowledge of the magnitude and temperature dependence of exchange splittings has frequently complicated analyses aimed at obtaining the relaxation frequency. A further reason for the present study was to determine a more accurate value of the constant $k = A_z/2hg_z$ utilizing the accurately known g_z value and a precise measurement of A_z obtained with improved Mössbauer resolution available to us. This determination should be possible since the relationship $\vec{g} = \text{const} \times \vec{A}$ holds[13] for an isolated Kramers state spanned by a single $\vec{J}$ such as the ground state of Dy^{3+} in $DyPO_4$. Further, we wished to use the Mössbauer technique as an independent method for measuring $g_\perp$ without the possible complications introduced by applying external magnetic fields. Once the constant k is known then $g_\perp = A_\perp/2hk$.

There have been no previous Mössbauer studies of hyperfine parameters in $DyPO_4$. A value of $|\frac{1}{2}A_z(^{161}\text{Dy})| = 2.565 \times 10^{-2}$ cm^{-1} (769 MHz) was deduced in the far-infrared (ir) work.[11] However, since the ground state of Dy^{3+} in $DyPO_4$ is almost pure $|J_z = \pm \frac{15}{2}\rangle$ we would expect a larger A_z parameter. Values as high as 800 MHz have been obtained in Mössbauer studies[14] of other dysprosium insulators. [The commonly used Mössbauer notation is $\frac{1}{2}A_z \equiv g_N\mu_N H_{\text{eff}} = (\mu_z/I)H_{\text{eff}}$ where H_{eff} is the "effective" magnetic field at the nucleus and μ_z is the ground-state nuclear magnetic moment.] Since the Mössbauer spectral resolution for the present study is a factor of 10 better than was the ir-laser resolution,[11] more accurate parameters can be determined. The nature of the ir study does not allow quadrupole P parameters to be determined. Prior to this work there had been no reported experimental observation, including Mössbauer, of $A_\perp$ contributions in spectra of dysprosium compounds.

With the resolution achieved in this study we could obtain the parameters A_z and $A_\perp$ as well as much of the information about the relaxation parameter $\Omega(T)$ by using scans of only the two components nearest zero Doppler velocity in the ^{161}Dy 16-line spectrum. There are obvious time-saving advantages to taking data in this manner. Also, independent calibrations using ^{57}Fe in standard absorbers can be made in this low-velocity range with high precision.

In Sec. II we discuss the crystalline electric field with emphasis on the Hamiltonian and wave functions appropriate to the D_{2d} point symmetry in $DyPO_4$. Relevant contributions to the magnetic and quadrupole hfs parameters for an isolated Kramers state are reviewed in Sec. III. A detailed analysis is given of the effects produced by $A_\perp$ on the eigenfunctions, eigenvalues, and transition probabilities for a combined nuclear and Kramers degenerate ionic state. The relationship $\vec{g} = K\vec{A}$ is developed and the relationship between the quadrupole interaction, various electronic shielding parameters, and the CEF Hamiltonian parameters are reviewed. Also, the relevant relaxation theory used in analyzing our spectra is developed in this section. A discussion of apparatus and procedure is given in Sec. IV. The experimental results are presented in Sec. V along with a calculation of the nuclear specific heat using our measured parameters for comparison with earlier anomalous results. A preliminary report of this work was presented by Forester and Ferrando.[15]

II. CRYSTALLINE ELECTRIC FIELD (CEF)

The free ion and crystal-field-split states[16] of Dy^{3+} are shown schematically in Fig. 2. The lowest multiplet, $^6H_{15/2}$, is separated by about 3000 cm^{-1} from the next multiplet. Within a good approximation, J of the ground manifold is a good quantum number although intermediate coupling corrections[17] will be used where appropriate throughout the text. The CEF strongly influences the ionic magnetic behavior, nuclear magnetic and nuclear quadrupolar hyperfine structure. Looking first at the ionic magnetic behavior and neglecting effects of nuclear hyperfine structure

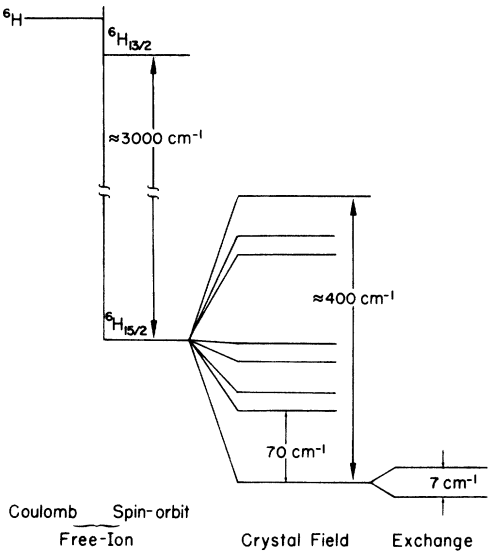

FIG. 2. Energy-level diagram for the Dy^{3+} ion in $DyPO_4$. The 7-cm^{-1} exchange splitting of the ground Kramers doublet represents the maximum splitting at $T=0$ K.

we write the ionic Hamiltonian

$$\mathcal{H}_{\text{ion}} = \mathcal{H}_0 \text{ (free ion)} + \mathcal{H}_{\text{crys}} + \mathcal{H}_{\text{exch}} + \mathcal{H}_{\text{Zeeman}} . \quad (1)$$

Within a single J manifold, $\mathcal{H}_{\text{crys}}$ of Eq. (1) may be expressed in terms of equivalent angular operators[18] $O_n^m(J_x, J_y, J_z)$:

$$\mathcal{H}_{\text{crys}} = \sum_{m,n} A_n^m \langle r^n \rangle_E \langle J \| \theta_n \| J \rangle O_n^m , \quad (2)$$

and $\langle J \| \theta_n \| J \rangle$ are the $\langle J \| \alpha \| J \rangle$, $\langle J \| \beta \| J \rangle$, and $\langle J \| \gamma \| J \rangle$ coefficients of Elliott and Stevens[13] for $n=2, 4$, and 6. Tables of matrix elements of O_n^m are given by Hutchings.[19] The products $A_n^m \langle r^n \rangle_E$ are usually considered as parameters to be determined experimentally.[20] However, in order to compare these with the parameters B_n^m deduced from optical experiments, a correction factor σ_n must be included to account for shielding of the $4f$ electrons by the $5s^2 5p^6$ electrons. This correction is usually written[21]

$$B_n^m = A_n^m \langle r^n \rangle_E (1 - \sigma_n) . \quad (3)$$

For a given configuration of Dy^{3+} in the D_{2d} symmetry of $DyPO_4$, Eq. (2) becomes

$$\mathcal{H}_{\text{crys}} = B_2^0 \langle J \| \alpha \| J \rangle O_2^0 + B_4^0 \langle J \| \beta \| J \rangle O_4^0 + B_6^0 \langle J \| \gamma \| J \rangle O_6^0 + B_4^4 \langle J \| \beta \| J \rangle O_4^4 + B_6^4 \langle J \| \gamma \| J \rangle O_6^4 . \quad (4)$$

For all symmetry lower than cubic, $\mathcal{H}_{\text{crys}}$ splits the ground $^6H_{15/2}$ state of Fig. 2 into eight twofold degenerate Kramers states.[22] The over-all CEF splitting is computed to be about 400 cm^{-1} based on estimates[16,23] of the crystal-field parameters in $DyPO_4$. These parameters are not expected to change appreciably for different rare-earth ions within the same local environment. A comparison between experimental parameters for[24] YPO_4:Er and estimates for $DyPO_4$,[23] based on limited information from low-lying CEF states, is given in Table I. In D_{2d} symmetry only eigenvectors which differ by $\Delta m_J = \pm 4$ enter. Thus, the ground Kramers state of $DyPO_4$ which is almost pure $|J_z = \frac{15}{2}\rangle$ is

$$|\Gamma_1^{\pm}\rangle = a|\pm\tfrac{15}{2}\rangle + b|\pm\tfrac{7}{2}\rangle + c|\mp\tfrac{1}{2}\rangle + d|\mp\tfrac{9}{2}\rangle . \quad (5)$$

$|\Gamma_1^+\rangle$ and $|\Gamma_1^-\rangle$ are degenerate in the absence of magnetic exchange or external magnetic field. Diagonalization of $\mathcal{H}_{\text{crys}}$ using the $DyPO_4$ parameters in Table I yields values of $a=0.986$, $b=-0.143$, $c=0.075$, and $d=0.044$.

The ground-state Kramers doublet in Fig. 2 has a maximum magnetic exchange splitting of about 7 cm^{-1} at $T=0$ K corresponding to a configuration with all four near-neighbor spins antialigned to the central ion spin. (See Fig. 1.) If one of the nearest-neighbor spins is reversed the exchange splitting is 3.5 cm^{-1} and if two are reversed the exchange splitting is zero.[8,9] This neglects the effects of spins other than first near neighbors, but such effects were not detected in the optical experiments.[16]

III. IONIC $\bar{g}$ TENSOR AND NUCLEAR HYPERFINE INTERACTIONS FOR A KRAMERS DOUBLET

A. $\bar{g}$ tensor

The Hamiltonian representing the interaction between an external field $\vec{H}_{\text{ext}}$ and the ionic magnetic moment $\vec{\mu}_e = \mu_B g_J \vec{J}$ is

$$\mathcal{H}_{\text{Zeeman}} = \mu_B g_J \vec{H}_{\text{ext}} \cdot \vec{J} , \quad (6)$$

where μ_B is the atomic Bohr magneton and g_J is the Landé factor. (With pure Russell-Saunders coupling $g_J = \frac{4}{3}$ for $^6H_{15/2}$, and with intermediate coupling corrections $g_J = 1.313$.[17]) For an isolated Kramers doublet, Eq. (6) may be written in the effective spin $S=\frac{1}{2}$ formalism,

$$\mathcal{H}_{\text{Zeeman}} = \mu_B \vec{H}_{\text{ext}} \cdot \bar{g} \cdot \vec{S} . \quad (7)$$

TABLE I. Comparison between experimental parameters for YPO_4:Er and estimates for $DyPO_4$. All entries are in units of cm^{-1}.

	B_2^0	B_4^0	B_6^0	B_4^4	B_6^4
$DyPO_4$ [a]	151.7	19.9	−44.2	−921	−97
YPO_4:Er [b]	141.4	18.1	−40.4	±837	±88.5

[a] Reference 23.
[b] Reference 24.

The magnetic properties of the ion, including anisotropy, are contained in the $\vec{\vec{g}}$ tensor which has components in a principal-axis system

$$g_z = 2g_J \langle \Gamma_1^+ | J_Z | \Gamma_1^+ \rangle ,$$
$$g_{x,y} = 2g_J \langle \Gamma_1^+ | J_{x,y} | \Gamma_1^- \rangle , \tag{8}$$

where $|\Gamma_1^+\rangle$ and $|\Gamma_1^-\rangle$ are the eigenfunctions of a Kramers state such as Eq. (5). The basis states of the spin $S=\frac{1}{2}$ Hamiltonian are $|\pm\frac{1}{2}\rangle$. For a pure $|J_z=\frac{15}{2}\rangle$ ground state the largest possible g_z from Eq. (8) is $g_z = 19.68$.

B. Magnetic nuclear hyperfine interactions

The nuclear magnetic hyperfine interaction Hamiltonian can be written

$$\mathcal{H}_m = (-)(\vec{N}_1+\vec{N}_2+\vec{N}_3)\cdot g_N\mu_N\vec{I}, \tag{9}$$

where $\vec{I}$ is the nuclear spin, and the nuclear g factor g_N is defined by $g_N\mu_N \equiv \mu_g/I$, where μ_g is the experimental nuclear moment and $\mu_N = 3.15 \times 10^{-12}$ eV/G.

The orbital contribution to the field, $\vec{N}_1$ is about 10^6–10^7 G for Dy^{3+}. $\vec{N}_2$ is the Fermi contact field equal to about -225 kG for Dy^{3+} in $DyPO_4$.[20] $\vec{N}_3$ represents all other contributions including direct interaction of $\vec{H}_{ext}$ with $\vec{I}$, dipolar, and exchange magnetic fields. In the present study $\vec{H}_{ext}=0$ and other terms in $\vec{N}_3$ are negligible compared with $\vec{N}_1$ and $\vec{N}_2$. Since both $\vec{N}_1$ and $\vec{N}_2$ are proportional to[20,25] $\vec{J}$ we follow analogous steps used to obtain Eqs. (7) and (8) to rewrite Eq. (9) in the spin $S=\frac{1}{2}$ formalism for an isolated Kramers doublet:

$$\mathcal{H}_m = \vec{I}\cdot\vec{\vec{A}}\cdot\vec{S}. \tag{10}$$

$\vec{\vec{A}}$ is the nuclear magnetic hyperfine tensor with principal-axis components of

$$A_z = 2a\langle \Gamma_1^+ | J_z | \Gamma_1^+ \rangle ,$$
$$A_{x,y} = 2a\langle \Gamma_1^+ | J_{x,y} | \Gamma_1^- \rangle , \tag{11}$$

where

$$a = -2\mu_B\mu_N g_N \langle 4f | r^{-3} | 4f \rangle \langle J \| N \| J \rangle + 90(g_J - 1)g_N\mu_N . \tag{12}$$

Comparing components of $\vec{\vec{A}}$ in Eq. (11) with components of $\vec{\vec{g}}$ in Eq. (8) for the same manifold then[13]

$$\vec{\vec{A}} = K\vec{\vec{g}}. \tag{13}$$

K may be evaluated experimentally using independently measured $\vec{\vec{g}}$ and $\vec{\vec{A}}$ tensor components. The most commonly tabulated ratio is

$$k \equiv K/2h = A_z/2hg_z = A_x/2hg_x = A_y/2hg_y . \tag{14}$$

Evaluation of K is important since it should allow determination of g_i with a measurement of A_i or vice versa for Dy^{3+} in any material when Eq. (13) applies. For extreme anisotropy ($A_x = A_y = 0$), Eq. (10) is usually discussed in terms of an "effective magnetic field"

$$H_{\text{eff}} = (A_z/g_N\mu_N)S_z \tag{15}$$

acting on the nuclear magnetic moment.

C. Nuclear quadrupole interaction

In principal-axis coordinates the nuclear quadrupole Hamiltonian is[26]

$$\mathcal{H}_Q = [e^2Q/(4I-1)] \times \{q_{zz}[3I_z^2 - I(I+1)] + q_{zz}\eta/2(I_+^2 + I_-^2)\} , \tag{16}$$

where Q is the nuclear quadrupole moment, q_{zz} is the axial electric field gradient at the nucleus, and $\eta \equiv (q_{xx} - q_{yy})/q_{zz}$ is the asymmetry parameter. For tetragonal symmetry $\eta = 0$.

The electric field gradient has a contribution from both the lattice CEF gradient and the nonspherical $4f$-electron charge distribution in a given ion. Equation (16) may be written

$$\mathcal{H}_Q = P[3I_z^2 - I(I+1)], \tag{17}$$

with

$$P = \frac{-e^2Q}{40}(1-R_Q)\langle 1/r^3 \rangle \langle J \| \alpha \| J \rangle \times \langle \Gamma_1^\pm | 3J_z^2 - J(J+1) | \Gamma_1^\pm \rangle \left(\frac{-e^2Q}{10}\right)\frac{B_2^0}{\langle r^2 \rangle}\ \frac{1-\gamma_\infty}{1-\sigma_2} . \tag{18}$$

The first term in P is the ionic contribution and the second term represents the lattice contribution[25] written in terms of B_2^0 [Eq. (4)], σ_2 [Eq. (3)], and R_Q and γ_∞ which are the ionic[27] and lattice[28] Sternheimer parameters.

D. Combined magnetic and quadrupole Hamiltonian

For the tetragonal symmetry of $DyPO_4$, $A_x = A_y \equiv A_\perp$. Combining Eqs. (10) and (17) the hfs Hamiltonian is

$$\mathcal{H}_{\text{hfs}} = A_z I_z S_z + \tfrac{1}{2}A_\perp(I^+S^- + I^-S^+) + P[3I_z^2 - I(I+1)]. \tag{19}$$

The eigenfunctions of $\mathcal{H}_{\text{hfs}}$ are linear combinations of product states involving both the nuclear and ionic basis functions. Thus, Mössbauer absorption takes place between the states

$$|a\rangle = \sum_{M_s, m_{I_g}} a(M_s, m_{I_g}) |\tfrac{1}{2}, M_s\rangle |I_g, m_{I_g}\rangle$$

and

$$|b\rangle = \sum_{M_s', m_{I_e}} b(M_s', m_{I_e}) |\tfrac{1}{2}, M_s'\rangle |I_e, m_{I_e}\rangle , \tag{20}$$

where $M_s, M_s' = \pm\frac{1}{2}$, $I_g = I_e = \frac{5}{2}$ for ^{161}Dy, and $m_I = \pm\frac{5}{2}$, $\pm\frac{3}{2}$, $\pm\frac{1}{2}$. The intensity of a particular transition is given by[29]

$$I_{ab}(\vec{k}) = P_a \left| \sum b(M_s', m_{I_e}) a(M_s, m_{I_g}) \times \langle M_s', m_{I_e} | \mathcal{H}_{\mathrm{Rad}}(\vec{k}) | M_s, m_{I_g} \rangle \right|^2 , \quad (21)$$

where $\sum$ indicates a summation over M_s', m_{I_e}, M_s, and m_{I_g}. $\mathcal{H}_{\mathrm{Rad}}(\vec{k})$ represents the multipole operator characteristic of the γ radiation involved and P_a is the probability of occupancy in the initial state. The dipole selection rules are $\Delta M_s = 0$, $\Delta m_I = 0, \pm 1$.

Eigenvalues and eigenvectors of Eq. (19) were derived and the allowed transition intensities were determined using Eq. (21) assuming a static electronic spin system, i.e., $\Delta M_s = 0$, during the nuclear transitions. The eigenvalues and allowed transitions are shown schematically in Fig. 3. With $A_\perp = 0$ there are 16 allowed transitions shown numbered on the left-hand side of Fig. 3 for $S_z = -\frac{1}{2}$ and an identical set of 16 transitions, not shown, corresponding to $S_z = +\frac{1}{2}$. Inclusion of $A_\perp$, however, produces admixtures of the $|M_s, m_I\rangle$ basis states, modifies the energy diagrams, and allows some previously forbidden transitions. Altogether there are 31 allowed transitions but many of these are too weak to be detected. Only one example is given in the center of Fig. 3; removal of the degeneracy of $|\frac{1}{2}, -\frac{1}{2}\rangle$ with $|-\frac{1}{2}, \frac{1}{2}\rangle$ leads to a doublet splitting of both lines 8 and 9 as shown schematically. Since $|\mu_e| > |\mu_g|$ in ^{161}Dy, line 8 will be split more than line 9 if $A_z < 0$. Thus, the magnitude of the doublet splittings is a measure of $A_\perp$ while the relative splitting of lines 8 and 9 provides the sign of A_z.

In Fig. 4 we show several computer-generated

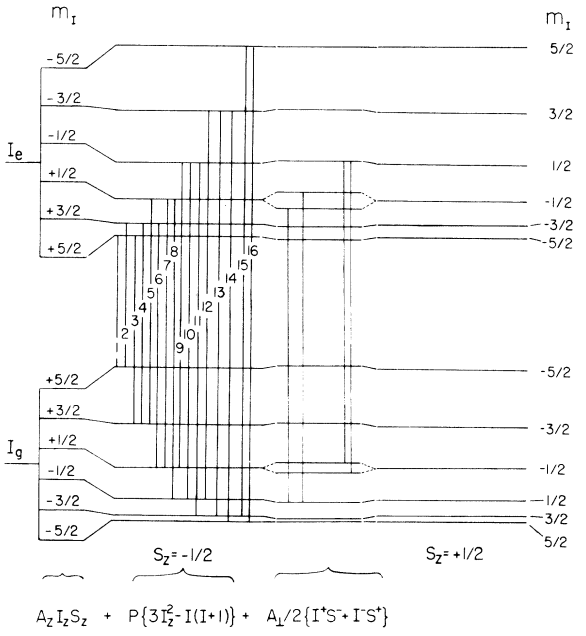

FIG. 3. Ground-state and excited-state nuclear energy levels and allowed transitions for ^{161}Dy in $DyPO_4$ assuming a Kramers degenerate ionic state. With $A_\perp = 0$ there are 16 allowed transitions for $S_z = -\frac{1}{2}$ as well as for $S_z = +\frac{1}{2}$ (these are not shown). With $A_\perp \neq 0$ there are 31 allowed transitions. Four of these are shown in the center of the diagram.

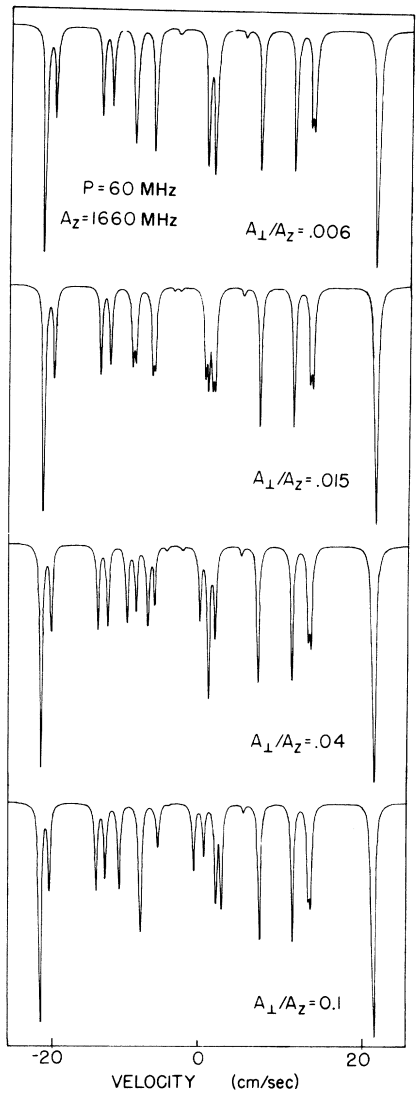

FIG. 4. Computer-generated ^{161}Dy spectra based on the diagram in Fig. 3. Kramers degeneracy is assumed. The parameters A_z and P are measured values for $DyPO_4$. Several small values of $A_\perp/A_z$ were chosen to show the dramatic effects on the spectra when $A_\perp \neq 0$.

absorption spectra for a powdered sample of $DyPO_4$ and *assuming Kramers degenerate states*. Values of $A_\perp/A_z = 0.006$, 0.015, 0.04, and 0.1 were chosen along with $A_z/h = -1660$ MHz and $P/h = 60$ MHz appropriate to $DyPO_4$ as discussed in Sec. V. The spectral resolution is that obtained in the present study. The dramatic splitting of lines 8 and 9 near zero velocity is evident. Although previous calculations of the type discussed above have been performed and computer-generated spectra have been illustrated,[14] these have concentrated on the region $A_\perp/A_z > 0.04$ since earlier experimental resolution did not allow smaller ratios to be observed.

E. Relaxation effects

There are a number of excellent papers and review articles[30-33] on the effects of electronic relaxation in Mössbauer spectra. Most of these treat the case in which $\mathcal{H}_{\rm hfs}$ in Eq. (19) is diagonal in $|M_s, m_I\rangle$. This is a good approximation for relaxation within a Kramers state for $g_z \gg g_x$, $g_y \cong 0$, or $A_\perp/A_z \cong 0$. The fluctuations may then be described by a time-dependent Hamiltonian[30]

$$\mathcal{H}_{\rm hfs}(t) = f(t) A_z I_z S_z + P[3I_z^2 - I(I+1)], \qquad (22)$$

where $f(t) = \pm 1$. As in Eq. (19), the magnetic and quadrupolar terms are taken to have the same principal axes. A treatment of the more complex problem including $A_\perp I^+ S^-$ terms has been given in the stochastic model by Clauser and Blume.[32] Although a more complete theoretical discussion of our data could be given using the latter treatment, the more complex analysis is not justified because of the smallness of $A_\perp$ in $DyPO_4$.

Relaxation information can be obtained from Mössbauer spectra only in the temperature interval between the fully collapsed high-temperature limit and the fully split static low-temperature limit. As for many dysprosium compounds this temperature interval for $DyPO_4$ extends well above T_N into the paramagnetic region. The necessary conditions for observation of *resolved* hfs in the *paramagnetic* region are[31] that (a) $\Gamma_n/\Omega_N < 1$ and (b) $\tau_e > 1/\Omega_N$, where τ_e is the relaxation-time parameter or correlation time ($\tau_e \equiv 1/\Omega$) and Ω_N is a frequency characteristic of the hyperfine interaction; $\Omega_N \sim A_i/\hbar$ for any i. In the case of extreme anisotropy $\Omega_N = \Omega_L$, the Larmor precession frequency

$$\Omega_L \equiv |g_N \mu_N H_{\rm eff}|/\hbar = |A_z|/2\hbar . \qquad (23)$$

When $\tau_e \sim 1/\Omega_N$ the spectra are no longer resolved and are quite broad and complex. For $\tau_e \ll 1/\Omega_N$ the magnetic hfs of a paramagnet collapses.

In $DyPO_4$, low-temperature relaxation is predominantly within the ground Kramers state. Since $g_\perp \cong 0$, spin-lattice relaxation is expected to be the dominant source of relaxation broadening. The relaxation treatment used in this paper assumes random spin reversals which produce random modulations of each allowed transition. This is equivalent to taking random fluctuations of $f(t)$ between ± 1 in Eq. (22).

Random modulation of a system of nuclear oscillators has been treated by various authors using different models.[30,33,34] Ultimately, the problem is to evaluate the "relaxation function" for the line shape. For a given frequency spectrum $I(\omega)$, a Fourier expansion may be written

$$I(\omega) = \mathrm{Re} \int_{-\infty}^{\infty} G(t) e^{-i\omega t}\, dt , \qquad (24)$$

where $G(t)$ is the "relaxation function" characterizing $I(\omega)$. The operator of interest for Mössbauer spectra is

$$G(t) = \exp\left(-i \int_0^t \omega_{m_I' m_I}(t')\, dt' \right), \qquad (25)$$

where $\omega_{m_I' m_I}(t) = \omega_{m_I'}(t) - \omega_{m_I}(t)$ is obtained from the time-dependent portion of $\mathcal{H}_{\rm hfs}$ in Eq. (22).

The central problem is the evaluation of Eq. (25). Our approach is the Anderson[35] stochastic model as developed for Mössbauer use by Blume.[36] Two summaries of the determination of $G(t)$ assuming stationary Markoffian processes are given by Abragam[34] and by van der Woude and Dekker.[31] The final result for $I(\omega)$ is

$$I(\omega) = -\mathrm{Re}\,(\vec{W} \cdot \mathfrak{A}^{-1} \cdot \vec{1})\, C(K), \quad K = 1, m \qquad (26)$$

where m is the number of Mössbauer spectral lines. The relative intensities $C(K)$ are obtained from the Clebsch-Gordan coefficients. $\vec{1}$ is a column vector with all entries equal to unity, $\vec{W}$ is the probability vector for the ionic states and is independent of time. The matrix $\mathfrak{A}$ is given by

$$\mathfrak{A} = i(\underline{\omega} - \omega \underline{E}) + \underline{\pi}, \qquad (27)$$

where $\underline{\pi}$ is the matrix of probabilities for Markoffian transitions between ionic states, ω is the frequency, $\underline{\omega}$ is the diagonal energy matrix of $\mathcal{H}_{\rm hfs}$, and $\underline{E}$ is the unit matrix.

For a Kramers doublet $|\Gamma_1^\pm\rangle$ we must consider two cases. The first case is a single degenerate state corresponding to zero exchange splitting ($\Delta_E = 0$). The probability of occupancy at any temperature T is the same for $|\Gamma_1^+\rangle$ and $|\Gamma_1^-\rangle$, i.e., $W_1 = W_2 = 1$. The second case is a nondegenerate doublet with $\Delta_E \neq 0$. In this case

$$W_1 \equiv p(-) = [1 + \exp(-\Delta_E/kT)]^{-1} \qquad (28)$$

and

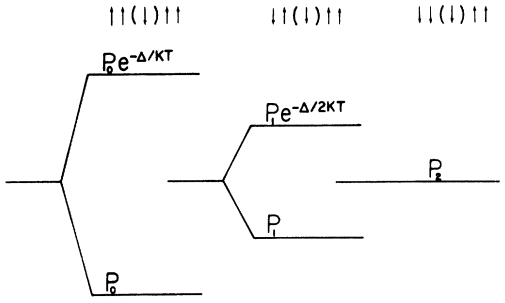

FIG. 5. Schematic representation of exchange splittings and their relative probabilities for the ground Kramers state of Dy^{3+} in $DyPO_4$. The parameter Δ is the maximum exchange splitting (7 cm^{-1}). The probabilities that a given ion will have four (P_0), three (P_1) or two (P_2) near-neighbors antialigned have been determined experimentally in Refs. 8 and 16.

$$W_2 \equiv p(+) = [1 + \exp(-\Delta_E/kT)]^{-1} \exp(-\Delta_E/kT). \tag{29}$$

In Eqs. (28) and (29), $\Delta_E = 7$, 3.5, or 0 cm^{-1} depending on whether four, three, or two nearest-neighbor magnetic moments are aligned antiparallel to the central Dy^{3+} moment.[8,16] These exchange splittings and their relative probabilities are shown schematically in Fig. 5. The temperature dependences of P_0, P_1, and P_2 are also known from earlier optical work.[8,16] We note that if the temperature at which relaxation first appears is such that $kT \gg \Delta_E$ then $W_1 \cong W_2$ in Eqs. (28) and (29), and one is justified in neglecting these exchange splittings.

IV. APPARATUS AND PROCEDURE

Mössbauer spectra were taken in transmission geometry using a constant-acceleration transducer driven in the triangular mode. Several different photon counters were used to detect the 26-keV ^{161}Dy γ rays. For this particular application, a krypton-filled proportional counter was found to out perform other gas and NaI scintillation counters. This provided an effective and inexpensive alternative[37] to solid-state detectors such as Li-drifted silicon. With a krypton-filled counter, the 26-keV peak is much better resolved from background x-ray escape peaks than for xenon-filled or NaI counters and the 13-keV escape peak of the Mössbauer γ ray is almost completely resolved. Data could then be taken with either the 26-keV or 13-keV peaks or both. Most of our data were taken with a single-channel analyzer setting which included both peaks. Counting rates were typically 10 000–20 000 counts/sec in the window.

The radioactive source was always maintained at room temperature. Calibrated platinum and germanium resistance thermometers were employed to measure and control the temperature. Temperature regulation was better than ±0.1 K, but temperature gradients across the sample produced an uncertainty at the absorber of about ±0.5 K. Runs at 1.8 K were made with the sample immersed in pumped liquid helium.

An isotopically enriched $(^{160}Gd_{0.5}\,^{162}Dy_{0.5})F_3$ source matrix was fabricated following the procedure of Cohen and Guggenheim.[38] ^{162}Dy enrichment was used to minimize the large neutron absorption cross sections from other Dy isotopes. No postirradiation annealing procedure was necessary and there was no indication of valence states other than Dy^{3+} in the source. The minimum room-temperature full-width-at-half-maximum (FWHM) linewidth observed, using the hyperfine-split absorption lines of $DyPO_4$ at 1.8 K was $\Gamma = 3.75$ mm/sec (77.5 MHz) or 0.0026 cm^{-1}. This is considerably larger than the natural linewidth ($2\Gamma_n = 0.38$ mm/sec) because of self-absorption within the source and residual unresolved quadrupole splitting in the source at room temperature. The linewidth is considerably less than those of Gd_2O_3 and GdF_3 ($\cdot nH_2O$) sources (FWHM ~10–20 mm/sec) which have been used for most ^{161}Dy Mössbauer studies to date although several recent experiments using dehydrated GdF_3 give comparable linewidths.

$DyPO_4$ single crystals were grown using the procedure of dissolution and reaction of rare-earth oxides in molten-lead pyrophosphates ($Pb_2P_2O_7$) at high temperatures with subsequent recrystallization of the rare-earth phosphate on cooling.[1,39] Crystals obtained in this growth were thin platelets with tetragonal c axes in the platelet plane. Several crystals of comparable thickness were carefully arranged to form a mosaic absorber approximately 0.5 in. in diameter and with an average of 7.5 mg/cm^2 of ^{161}Dy. Another absorber was prepared by grinding several single crystals into powder and then pressing these into an organic binder containing about 11.5 mg/cm^2 of ^{161}Dy.

The Mössbauer spectra were least-squares analyzed by computer using various theoretical routines developed to calculate the absorption cross sections in the case of off-diagonal hyperfine interaction, relaxation, polarized γ-ray spectra, etc.

Data were taken in three velocity ranges corresponding roughly to ±2.5, ±8.33, and ±25 cm/sec. Calibration in the ±2.5-cm/sec range was made quite precisely using an ^{57}Fe-enriched α-Fe_2O_3 absorber and a ^{57}Co-in-copper source, both at room temperature. Extension of this calibra-

tion to higher velocity ranges can produce sizeable error and considerable care was exercised. In practice we first took spectra of $DyPO_4$ in the ±2.5-cm/sec range at $T = 1.8$ K. Using the above Fe_2O_3 calibration, the spacing between lines 8 and 9, $\Delta(9-8)$ (see Fig. 3), was determined. At 1.8 K any $A_\perp$ hyperfine contributions are suppressed and $\Delta(9-8)$ is dependent only on A_z through the expression

$$\Delta(9-8) = \tfrac{1}{2}(|\mu_e/\mu_g| - 1)A_z . \quad (30)$$

Inserting our measured $\Delta(9-8)$ into Eq. (30) and using the precisely measured[40] $|\mu_e/\mu_g| = 1.241 \pm 0.004$, the parameter $A_z = 2\mu_g H_{\text{eff}}$ was determined. Next, a full 16-line spectrum was taken at low temperature over the ±25-cm/sec velocity range. The separation between peaks 1 and 16 is

$$\Delta(16-1) = [(|\mu_e/\mu_g| + 1)/(|\mu_e/\mu_g| - 1)]5\Delta(9-8) . \quad (31)$$

Using $\Delta(9-8)$ and $|\mu_e/\mu_g|$ from above, the velocity calibration was determined for the ±25-cm/sec range.

V. EXPERIMENTAL RESULTS

Prior to introducing the data, it is useful to summarize our analysis procedure. This was carried out in three temperature ranges: (i) For $T < 3K$, almost all Dy^{3+} ions experience the maximum near-neighbor exchange field. That is, each Dy^{3+} spin has four oppositely directed near-neighbor spins (Fig. 5). All Kramers degeneracy is lifted, and off-diagonal $A_\perp$ contributions in Eq. (19) are quenched. The resultant 16-line absorption spectrum is just a superposition of the 16 lines indicated in Fig. 3 for $S_z = +\frac{1}{2}$ and those for $S_z = -\frac{1}{2}$. There was no observed relaxation contribution in this region and $f(t)$ in Eq. (22) was therefore taken to be unity. (ii) For $3 \lesssim T \lesssim 10$ K there was still no observed relaxation and the static hyperfine treatment with $f(t) = 1$ was used. However, as observed by Wright *et al.*,[8,16] above about 3 K some ions experience zero net exchange splitting. Appropriate eigenvalues must be calculated for these ions with Eq. (19) including $A_\perp$ terms. Therefore, spectra in this region were computed by superimposing spectra corresponding to ions with and ions without Kramers degeneracy and using weighting factors determined by Wright *et al.* for the two cases. (iii) Above 10 K, relaxation effects were clearly observed, and a time dependence $f(t)$ was included in Eq. (22) using the stationary-Markoffian-process relaxation treatment of Sec. IV. The ground- and excited-state hyperfine parameters determined for $T < 3$ K were assumed to remain the same at higher temperatures. This assumption is valid up to about 60 K at which point population of the CEF states near 108 K begins to contribute. As discussed in Sec. III, the time-dependent calculation for $10 \lesssim T \lesssim 60$ K has only one parameter, the relaxation frequency $\Omega(T)$, to be determined. The exchange gaps and probabilities of their occurrence as a function of temperature are included in the calculation as fixed parameters (see Sec. III E).

A. Spectral analysis for $T \lesssim 3$ K

Representative spectra for $T \lesssim 3$ K are shown in Figs. 6–8. In Fig. 6, the entire 16-line spectrum for a single-crystal sample at $T \simeq 3$ K is plotted. The direction of γ-ray propagation was perpendicular to the tetragonal c axis of the crystal. Spectra in Fig. 7 were taken in the lower, ±2.5-cm/sec, velocity range using a powdered absorber of $DyPO_4$. Only lines 8 and 9 of Fig. 3 are observable in this velocity range. The 1.8- and 3.5-K spectra from Fig. 7 are shown on an expanded scale in Fig. 8 to display subtle differences in the observed spectral shapes for the two temperatures.

In Fig. 7 the separation between peaks, $\Delta(9-8)$, at 1.8 K is given by Eq. (30). The solid curve drawn through the data is the result of a Lorentzian least-squares curve-fitting analysis using A_z, the spectral centroid, peak widths, and peak depths as independent parameters. This analysis yields $\Delta(9-8) = 9.69 \pm 0.03$ mm/sec from which we obtain $|A_z/h| = 1662 \pm 9$ MHz or $|\mu_g H_{\text{eff}}/h| = 831 \pm 4$ MHz for the ^{161}Dy ground state in $DyPO_4$. The value of A_z is somewhat larger than those obtained in other dysprosium insulators, Table II, and is consistent with the almost pure $|J_z = \frac{15}{2}\rangle$ ionic ground state [see Eq. (13)]. Interestingly, it is almost identical to A_z obtained by NMR for ^{161}Dy in dysprosium metal.[42] It is equivalent to an effective magnetic field $H_{\text{eff}} = 5.8$ MG. From this we estimate the free Dy^{3+} ion field to be H_{eff} (ion) $= [g_z(\text{ion})/g_z(DyPO_4)]H_{\text{eff}}(DyPO_4) = (19.68/19.3) \times 5.8$ MG or H_{eff} (ion) $= 5.9$ MG (847 MHz). The only previous attempt to determine A_z for $DyPO_4$ was made using far-infrared EPR.[11] This result shown in Table II is about 7% lower than our Mössbauer result. Using[11] $g_z = 19.32 \pm 0.01$ for $DyPO_4$ we compute from Eq. (14) the factor $k = A_z/2hg_z = 43.0 \pm 0.2$ (in MHz). The differences between the far-infrared EPR values for A_z (and k) and the Mössbauer values are too great to be attributable to experimental uncertainties. It should also be noted that the measurements of Prinz *et al.*[15] determined both A_z and g_z by the same technique and not just their ratio. Since this is the first time precision measurements of A_z have been made on the same material by independent

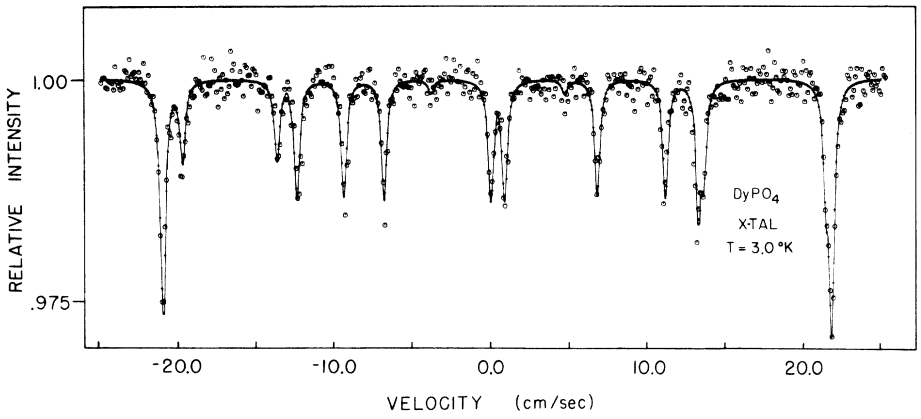

FIG. 6. Mössbauer transmission spectrum of ^{161}Dy in a $DyPO_4$ single crystal at $T = 3$ K. The direction of γ-ray propagation was perpendicular to the tetragonal c axis.

techniques (one measuring hfs on the ionic energy levels and the other measuring hfs at the nucleus) the discrepancies were totally unexpected. It is usually assumed that the magnitudes of the ionic and nuclear hfs should be the same. To our knowledge, however, this has not been proven either experimentally or theoretically.

In Fig. 6 the over-all spectral splitting was determined to be $\Delta(16-1) = 450 \pm 3$ mm/sec by substituting A_z obtained above into Eq. (31). The solid

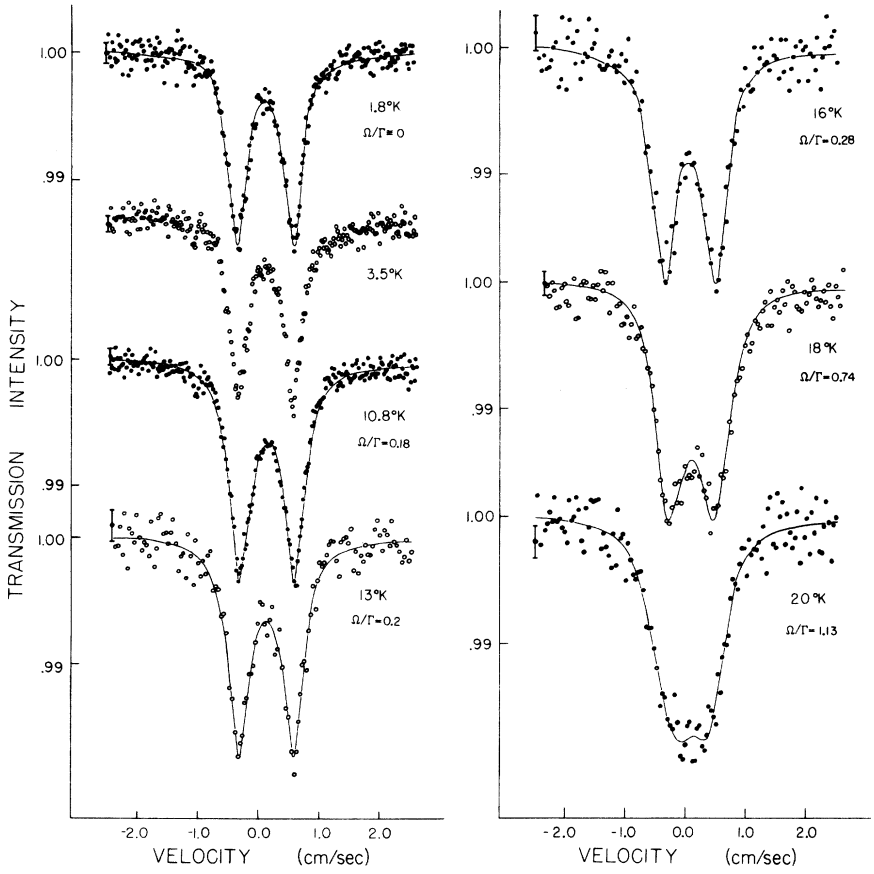

FIG. 7. Mössbauer transmission spectra for a powdered $DyPO_4$ absorber. Only the two lines nearest zero velocity are shown in these scans. The solid curves are computer least-squares fits to the data for the relaxation frequency to linewidth ratios Ω/Γ shown.

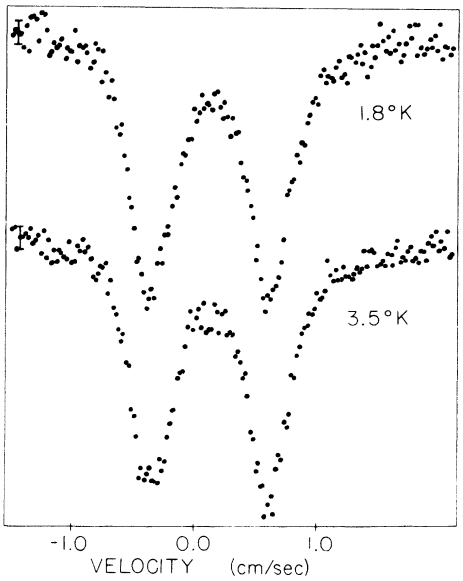

FIG. 8. Expanded plot of the $T = 1.8$ and 3.5 K spectra of Fig. 7 showing the subtle differences in line shapes and peak positions observed in this temperature region.

curve through the data is the result of least-squares analysis using the quadrupole parameters P_e and P_g, the spectral centroid, and the peak intensities as variable parameters. All linewidths were assumed equal and it was assumed that $A_\perp = 0$ for this analysis. Values of $P_e/P_g = 0.986 \pm 0.003$, $P_g/h = 60.3 \pm 0.6$ MHz and $P_e/h = 59.5 \pm 0.6$ MHz were obtained. These are compared with results on other Dy compounds in Table II. The ratio P_e/P_g could be computed more accurately than either P_e or P_g separately since the latter computation depends on the calibration accuracy while the former does not. Small differences were detected between the measured relative intensities in Fig. 6 and calculated intensities using the Clebsch-Gordan coefficients and angular factors. These differences are attributed to finite-thickness effects which were not incorporated in the analysis. Presumably at $T = 3$ K there could also be intensity changes because of $A_\perp$ contributions to part of the spectrum. As discussed below, however, these effects are too small to be observable within the statistical fluctuations of the data obtained in the full-spectrum scans. In the computer analysis the intensities were allowed to deviate slightly from their theoretical values but peaks with equal theoretical intensities were constrained to have equal amplitudes.

B. Spectral analysis for $3 \lesssim T \lesssim 10$ K

The 1.8- and 3.5-K spectra in Fig. 8 are representative of a number of spectra taken in this temperature range. At the lowest temperature, both peaks of the doublet spectra have the same widths and depths. As the temperature was raised, however, a subtle difference in spectral shape exemplified by the 3.5-K spectrum was noted. A careful analysis of the two spectra in Fig. 8 also reveals extremely small differences in the mean centroid of corresponding peaks and the separation between these mean centroids. Since there is no experimental evidence to indicate a lattice distortion or anomalous behavior in $DyPO_4$ at these temperatures,[6] we interpret the asymmetrical line shapes in terms of off-diagonal hfs as discussed in

TABLE II. A comparison of experimental ^{161}Dy hyperfine parameters for several different materials. The parameters $-\mu_g H_{\rm eff}/h$, P_g/h, and k are all in MHz. All entries except those noted are from Ref. 14. All k values are calculated ratios of g_i/A_i. Entries in parentheses are calculated values; e.g., g_z for DyES is computed from available crystal-field parameters, the ionic parameters are computed for a pure $|J_z = \frac{15}{2}\rangle$ state while the other "calculated" g_z's are deduced using the measured $\mu_g H_{\rm eff}/h$ parameters and the k ratios listed.

Material	$-\mu_g H_{\rm eff}/h$	μ_e/μ_g	μ_g	P_e/P_g	P_g/h	g_z	$g_\perp$	k
Dy^{3+} ion	(847 [a])		0.47± 0.09 [b]		(72.8 [a])	(19.68)		43 [a]
Dy metal	831± 1 [c]	−1.241± 0.004 [f]		1.01 ± 0.03	64.4± 0.3 [c]	(19.7)		42± 2
$DyPO_4$	831± 4 [d]			0.986± 0.003 [d]	60.3± 0.6 [d]		0.3± 0.1 [d]	43.0± 0.2 [d]
$DyPO_4$	769 [e]					19.32± 0.01 [e]	0.7± 0.1 [e]	39.8 [e]
$DyPO_4 \cdot 5H_2O$	795				57.5	(18.8)		42.3± 1
$Dy_2(MoO_4)_3$	799				50.0	(18.9)		42.3± 1
DyES	446± 12				15.8± 0.5	(10.75)		41.6± 1
DyA1G	769± 15	−1.21± 0.02		0.98 ± 0.03	37	(18.2)		42.2± 1

[a] Calculated in this study.
[b] Reference 41.
[c] Reference 42.
[d] Mössbauer (this study).
[e] Far-infrared EPR—Ref. 11.
[f] Reference 40.

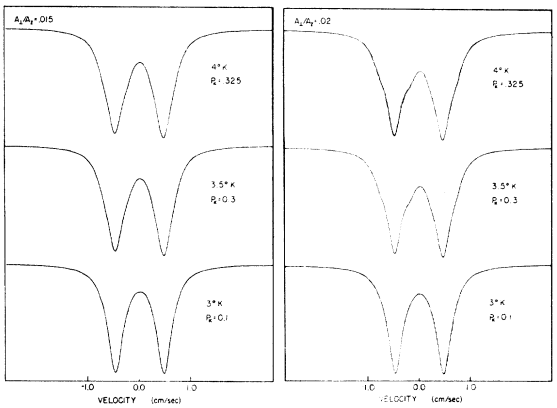

FIG. 9. Computer generated Mössbauer spectra near zero velocity. These were calculated using a superposition of spectra for $A_\perp \neq 0$ (weight P_K) and $A_\perp = 0$ (weight $1 - P_K$). The fraction P_K of Kramers degenerate ions in $DyPO_4$ vs temperature has been determined experimentally in Refs. 8 and 16.

Sec. III. As shown below, the magnitude of $A_\perp$ deduced from this asymmetry is consistent with the small $g_\perp$ expected in $DyPO_4$. Earlier in Fig. 4 we generated spectra for various ratios of $A_\perp/A_z$ assuming a *degenerate* Kramers ionic state. Clearly, the effects of a quite small $A_\perp$ should be conspicuous. However, at very low temperatures, $A_\perp$ terms are quenched by removal of the Kramers degeneracy as discussed in Sec. III. At higher temperatures a fraction P_k are degenerate and $1 - P_k$ are nondegenerate.[8,16] Thus, the effects of $A_\perp$ must be calculated using a superposition of spectra for $A_\perp \neq 0$ (weight P_k) and $A_\perp = 0$ (weight $1 - P_k$). This superposition was calculated for the central doublet at temperatures of 3 K, 3.5 K, and 4 K and the generated spectra are shown in Fig. 9. Two representative ratios $A_\perp/A_z = 0.015$ and 0.02 were chosen. Spectra generated with either higher or lower ratios were in gross disagreement with the data. Values of P_k deduced from the data of Wright *et al.*[8,16] are indicated in Fig. 9. From a comparison of these calculated curves with the 3.5 K spectrum in Fig. 8 we deduce $A_\perp/A_z = 0.017 \pm 0.005$. Taking the value of[11] $g_z = 19.32 \pm 0.01$ we deduce $g_\perp = (A_\perp/A_z)\, g_z = 0.3 \pm 0.1$. This is certainly within the range $g_\perp = 0.5 \pm 0.5$ first reported by Wright *et al.*[9] but is smaller than the more recent[11] $g_\perp = 0.7 \pm 0.1$ deduced from far-infrared EPR work. The infrared spectra were complicated by a number of overlapping spectra from different isotopes and the experimental spectra had to be theoretically corrected to remove extensive broadening effects due to a large nonuniform demagnetizing field within the sample. These difficulties probably account for the differences in $g_\perp$ obtained by the two experimental techniques. We note two possible mechanisms which could make the $A_\perp$ contribution in our Mössbauer study appear to be smaller than it actually is. One of these is possible exchange splittings due to ions more distant than first nearest neighbors. There was no evidence for this in earlier zero-field optical work.[16] A second possible mechanism is relaxation broadening at temperatures below 10 K. This would tend to average out the calculated differences in spectra for Kramers degenerate and nondegenerate ions. The observed temperature-dependent line shapes below

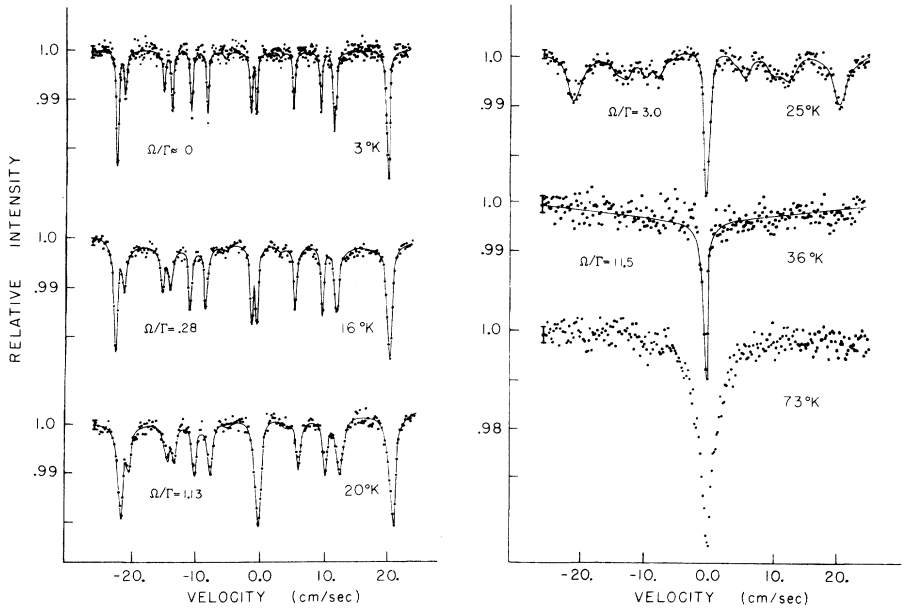

FIG. 10. Mössbauer transmission spectra in $DyPO_4$. The 3-K spectrum was taken with a single-crystal sample. The remainder were taken with powdered samples. Again the solid curves are computer fits to the data.

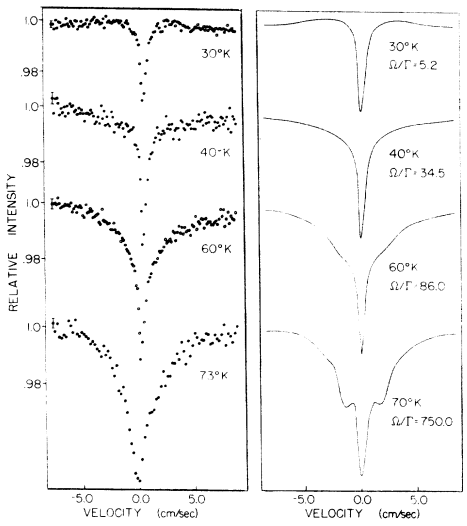

FIG. 11. Mössbauer transmission spectra and calculated spectra for the temperature range $T = 30$ to $T \cong 70$ K. Note the reduced velocity scan from Fig. 10. The calculated spectra do not agree with the data above $T = 60$ K because of population and relaxation through excited crystal-field states near 70 cm^{-1} (108 K).

10 K are not consistent with this mechanism at least within the relaxation model we have assumed. At this point we feel that $g_\perp$ inferred from our Mössbauer study is certainly a lower limit while the infrared value represents an upper limit. We also feel that the Mössbauer $g_\perp$ is more representative of the true zero-field value.

C. Spectral analysis for $T > 10$ K

Representative spectra for the region $T > 10$ K are plotted in Figs. 7, 10, and 11. Relaxation broadening begins abruptly near $T = 10$ K and increases sharply with increasing temperature. The solid curves shown in Figs. 7, 10, and 11 are the result of analysis using the Ising relaxation treatment discussed in Sec. III E. The time evolution of the spectra is described by Eq. (26) and the low-temperature hyperfine parameters are assumed to be independent of temperature. Ratios of Ω/Γ associated with the computer fittings are shown in Figs. 7, 10, and 11 where Γ is the minimum observed absorption linewidth; $\Gamma = 77.5$ MHz. From Table II the Larmor frequency associated with A_z is $\Omega_L = 831$ MHz. The calculated Ω/Γ values indicate that $\Omega \cong \Omega_L$ near $T = 36$ K. The minimum detectable frequency was 14 MHz near and below 10.8 K. Although the relaxation rate certainly continues to decrease below 10.8 K, it could not be followed because of the source linewidth. Note that the hyperfine structure is still well resolved for $T \gg T_N = 3.39$ K. At $T = 60$ K the frequency is 6670 MHz. Above this temperature our theoretical analysis based on a single relaxation frequency within a single Kramers state could not reproduce the experimental spectra. This is because other states near 70 cm^{-1} (108 K) are being populated (see Fig. 2). This alters the relaxation channels and produces a superposition of more than one hyperfine spectrum. A comparison of the experimental and calculated spectra near $T = 70$ K in Fig. 11 indicates that quadrupole splittings associated with these states near 70 cm^{-1} are considerably smaller than for the ground Kramers state. In Fig. 12 the Ω/Γ values are plotted on a log scale versus $1/T$. Below $T \simeq 36$ K the data fall on a straight line. This temperature dependence is characteristic of spin-lattice relaxation proceeding by an Orbach process.[43] The transition between the $|\Gamma_1^+\rangle$ and $|\Gamma_1^-\rangle$ components of the ground, exchange-split Kramers state is thus an indirect scattering process involving an excited electronic state at Δ_G above the ground state with $\Omega = \Omega_0 e^{-\Delta_G/T}$. From the slope of the straight line in Fig. 12 we obtain $\Delta_G \cong 110$ K which is in close agreement with the calculated position of the first excited crystal-field state in $DyPO_4$.[10,11] A value $\Omega_0 = 2 \times 10^{10}$ sec^{-1} is also deduced from Fig. 12.

The dashed curve in Fig. 12 is from data taken by Gorebchenko *et al.*[44] on $DyVO_4$. Over the limited temperature range of 4–11 K they also observe a linear dependence on $1/T$ with an associated $\Delta_G = 40$ K. However, the relaxation processes in $DyVO_4$ are complicated by a crystallographic transition at $T \cong 13$ K.

We note here that although the experimental exchange gaps were incorporated into our analysis through Eqs. (28) and (29), they have little influence on the observed relaxation (compared with

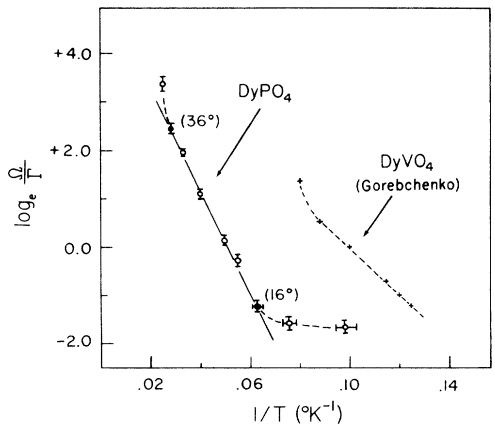

FIG. 12. Temperature dependence of spin-lattice relaxation frequencies determined from our Mössbauer data on $DyPO_4$ and that of Gorebchenko *et al.* (Ref. 44) on $DyVO_4$.

taking $W_1 = W_2$) except at temperatures near 11 K. This is because the maximum exchange gap is about 10 K and for $kT \gg \Delta E$, Eqs. (28) and (29) reduce to $W_1 = W_2$.

D. Quadrupole and shielding parameters

The first term in Eq. (18) is the $4f$-orbital contribution to the quadrupole parameter P. The factor R_Q in this equation is a number much smaller than one and most estimates yield roughly the same value for it. We use $R_Q = 0.124$ from the theoretical calculations of Gupta *et al.*[45] Using $|\Gamma_1\rangle$ from Eq. (5), $Q = (2.36 \pm 0.04) \times 10^{-24}$ cm^2,[41] $\langle r^{-3} \rangle = 62.087 \times 10^{24}$ cm^{-3},[46] and $\langle J \| \alpha \| J \rangle = -0.066\,215$ we calculate the ionic contribution to P: P_{ion}/h ($DyPO_4$) = 70.4 MHz. This is greater than the measured value of 60.3 MHz because the lattice contribution to P [the second term in Eq. (18)] has the opposite sign to P_{ion}. From the calculated P_{ion} we estimate the lattice contribution: $P_{\text{lat}} = P_{\text{meas}} - P_{\text{ion}}$ or P_{lat}/h ($DyPO_4$) = − 10 MHz.

Information concerning electric field gradient shielding parameters is frequently inferred from P_{lat}. From Eq. (18)

$$P_{\text{lat}} = -(e^2 Q B_2^0 / 10 \langle r^2 \rangle)[(1 - \gamma_\infty)/(1 - \sigma_2)]. \quad (32)$$

Taking $B_2^0 = 151.7$ from Table I, $\langle r^2 \rangle = 0.203 \times 10^{-16}$ cm^2,[20] and Q and P_{lat} from above, we calculate

$$\alpha \equiv (1 - \gamma_\infty)/(1 - \sigma_2) = 190. \quad (33)$$

This is very close to the theoretical α calculated by Gupta *et al.*[45] for Dy^{3+}. Wickman *et al.*[47] determine $\alpha = 262$ in DyES. However, they used an earlier, less accurate, value of $Q = 2.6 \times 10^{-24}$ cm^2.[48] If the more recent Q is used instead then their α is in close agreement with our own. However, DyES is a much better material in which to study the ratio α since P_{lat} is almost five times larger than in $DyPO_4$. It will be interesting to remeasure this parameter in DyES using a higher resolution fluoride source similar to that used in the present study.

E. Nuclear specific heat

In an earlier specific-heat measurement, Colwell *et al.*[2,9] obtained a value for the nuclear specific-heat contribution of $C_N T^2/R = 0.000\,33$ K^2 based on data between $T = 0.4$ and 0.6 K. They themselves questioned this result since it is a factor of 10 smaller than that calculated using the expansion term

$$C_N T^2/R \cong (A_z^2/9)[S(S+1)][I(I+1)].$$

From the present Mössbauer results, the nuclear energy levels E_i of Fig. 3 appropriate to ^{161}Dy can be calculated. With the measured ratios[41] $A_z(^{163}\text{Dy})/A_z(^{161}\text{Dy}) = -1.404$ and $P(^{163}\text{Dy})/P(^{161}\text{Dy}) = 1.04$, the energy-level diagram for ^{163}Dy can also be calculated. Only ^{161}Dy and ^{163}Dy contribute to the nuclear specific heat. All the other isotopes are even-even and have degenerate nuclear states. The relative abundances of these isotopes is known to be ^{163}Dy : ^{161}Dy : Dy (even-even) = 24.9 : 18.7 : 56.4.[11] With this information the nuclear specific heat can be calculated for each isotope and then summed to get the total using[49]

$$C_N = \frac{R}{(kT)^2}\left(\sum_{i=-I}^{I}\sum_{j=-I}^{I}(E_i^2 - E_i E_j)e^{-(E_i+E_j)/kT}\right)\Big/\sum_{i=-I}^{I}\sum_{j=-I}^{I}e^{-(E_i+E_j)/kT}. \quad (34)$$

Wright *et al.*[9] ignored the quadrupole contribution P. The inclusion of the P term in our calculation has a marked effect on the shape and location of the Shottky anomaly near $T = 0.04$ K. However, $C_N T^2/R$ is reduced by only 10% in the range $0.4 \leq T \leq 0.6$ K which is the range of the measured specific heats. Therefore, a first-principle calculation of C_N using measured nuclear parameters cannot account for the anomalously low specific heat observed by Wright *et al.*[9] It seems likely, as they speculate, that a thermal contact problem caused spurious results at the lowest temperatures of their study.

VI. CONCLUSION

Mössbauer spectroscopy of the 26-keV γ-ray transition in ^{161}Dy has been employed to study nuclear hyperfine interactions in the Ising-like antiferromagnet $DyPO_4$. The spectral resolution available allowed accurate determination of the magnetic hyperfine tensor components and relaxation-frequency parameter from low-velocity scans of the central doublet in the 16-line spectra. The value of A_Z determined is about 7% higher than that obtained in previous far-infrared EPR experiments[11] and is very close to the calculated A_Z for a free Dy^{3+} ion. Since this is the first time precision measurements of this parameter have been made on the same material by independent techniques (involving ionic hfs and nuclear hfs) the discrepancies were totally unexpected and raise interesting questions regarding the assumptions upon which previous hyperfine data analysis has been based. A new value for $k = A_z/2hg_z$ was

determined with greater accuracy than previous experiments. Likewise, an improved value for the ratio of excited-state to ground-state quadrupole moments Q_e/Q_g was deduced. The lattice contribution to the quadrupole interaction was determined after calculating the ionic contribution using the ground state Dy^{3+} wave function obtained in infrared and optical studies.[16,23] From this lattice contribution a ratio of shielding parameters $(1-\gamma_\infty)/(1-\sigma_2)$ was calculated which is in good agreement with other theoretical[45] and experimental work.[47] The effect of off-diagonal $A_\perp$ contributions to ^{161}Dy spectra was observed for the first time but only in a temperature window $3 \lesssim T \lesssim 10$ K. At very low temperatures almost all Dy^{3+} ions have their Kramers degeneracy lifted by near-neighbor exchange coupling and the $A_\perp$ contributions are quenched. Between $T=3$ and 10 K an increasing number of ions see a zero net exchange field from antialigned near neighbors and are Kramers degenerate. The fraction of ions with and without Kramers degeneracy is available from optical data[8,16] and was included in our analysis. From the measured $A_\perp$ a value for $g_\perp = A_\perp/2hk = 0.3 \pm 0.1$ was computed. This is somewhat lower than $g_\perp = 0.7 \pm 0.1$ reported in recent infrared[11] work done in high magnetic fields. Since there are possible reasons for error in either experimental technique, the true value of $g_\perp$ is presumed to be between the lower limit established by Mössbauer work and the upper limit established by infrared work. Either number establishes an extremely high anisotropy of the $\tilde{g}$ tensor. Relaxation contributions to the spectra were analyzed in the Anderson[35] stochastic model as developed for Mössbauer use by Blume.[36] By incorporating exchange splittings of the ground Kramers doublet determined from optical studies[8,16] the spectra could be analyzed using a single relaxation-frequency parameter $\Omega(T)$. Values of Ω were determined for $11 \lesssim T \lesssim 60$ K. For $16 \lesssim T \lesssim 36$ K the temperature dependence is $\Omega = \Omega_0 e^{-\Delta_G/T}$ corresponding to an Orbach[43] spin-lattice relaxation process via an excited electronic state at Δ_G. The Δ_G obtained in this analysis is in close agreement with that deduced in far-infrared studies.[10,11] The nuclear specific heat for $DyPO_4$ was calculated from first principles using the measured nuclear parameters obtained in this study. This calculation showed that the $C_N T^2/R$ deduced in low-temperature specific-heat measurements[2] is a factor of 10 too small.

---

*Present address: Physics Department, American University, Washington, D. C.

†Supported by a NRL-NRC Research Postdoctoral fellowship.

[1]These crystals were taken from the same growth series as those used for magneto-electric (Ref. 7) and far-infrared EPR studies (Refs. 10 and 11).

[2]J. H. Colwell, B. W. Mangum, D. D. Thornton, J. C. Wright, and H. W. Moos, Phys. Rev. Lett. 23, 1245 (1969).

[3]R. W. G. Wyckoff, *Crystal Structures*, 2nd ed. (Interscience, New York, 1965), Chap. VIII.

[4]H. Schwarz, Z. Anorg. Allg. Chem. 323, 44 (1963).

[5]H. Fuess, A. Kallel, and F. Tcheon, Solid State Commun. 9, 1949 (1971).

[6]W. Scharenberg and G. Will, Int. J. Magn. 1, 277 (1971).

[7]G. T. Rado, Phys. Rev. Lett. 23, 644 (1969).

[8]J. C. Wright and H. W. Moos, Phys. Lett. A 29, 495 (1969).

[9]J. C. Wright, H. W. Moos, J. H. Colwell, B. W. Mangum, and D. D. Thornton, Phys. Rev. B 3, 843 (1971).

[10]G. A. Prinz and R. J. Wagner, Phys. Lett. A 30, 520 (1969).

[11]G. A. Prinz, J. L. Lewis, and R. J. Wagner, Phys. Rev. B 10, 2907 (1974).

[12]M. F. Sykes, J. W. Essam, and D. S. Gaunt, J. Math. Phys. 6, 283 (1965).

[13]R. J. Elliott and K. W. H. Stevens, Proc. R. Soc. A 218, 553 (1953).

[14]H. H. Wickman and I. Nowik, J. Phys. Chem. Solids 28, 2099 (1967).

[15]D. W. Forester and W. A. Ferrando, AIP Conf. Proc. 18, 523 (1974).

[16]J. C. Wright, Ph. D. dissertation (Johns Hopkins University, 1970) (unpublished), available from University Microfilms, Inc., Ann Arbor, Mich.

[17]B. G. Wybourne, J. Chem Phys. 36, 2310 (1962).

[18]R. Orbach, Proc. R. Soc. A 264, 458 (1961).

[19]M. T. Hutchings, Solid State Phys. 16, 227 (1966).

[20]A. J. Freeman and R. E. Watson, Phys. Rev. 127, 2058 (1962).

[21]Gerald Burns, J. Chem. Phys. 42, 377 (1965).

[22]W. Low, *Paramagnetic Resonance in Solids* (Academic, New York, 1960), p. 34.

[23]Joan L. Lewis and G. A. Prinz (private communication).

[24]Dieter Kuse, Z. Phys. 203, 49 (1967).

[25]S. Ofer, I. Nowik, and S. G. Cohen, *Chemical Applications of Mössbauer Spectroscopy*, edited by V. I. Goldanskii and R. H. Huber (Academic, New York, 1968), Chap. VIII, and references therein.

[26]R. G. Barnes, R. L. Mössbauer, E. Kankeleit, and J. M. Poindexter, Phys. Rev. 136, A175 (1964).

[27]R. M. Sternheimer, Phys. Rev. 84, 244 (1951).

[28]R. M. Sternheimer, Phys. Rev. 132, 1637 (1963).

[29]H. H. Wickman, M. P. Klein, and D. A. Shirley, Phys. Rev. 152, 345 (1966), and references therein.

[30]M. Blume and J. A. Tjon, Phys. Rev. 165, 446 (1968), and references therein.

[31]F. van der Wöude and A. J. Dekker, Phys. Status Solidi 9, 977 (1965).

[32]M. J. Clauser and M. Blume, Phys. Rev. B 3, 583 (1971).

[33]S. Hufner, H. H. Wickman, and C. E. Wagner, Phys. Rev. 169, 247 (1968).

[34]A. Abragam, *The Principles of Nuclear Magnetism* (Clarendon, Oxford, 1961), p. 447.
[35]P. W. Anderson, Phys. Rev. 76, 471 (1949).
[36]M. Blume, Phys. Rev. Lett. 14, 96 (1965).
[37]D. W. Forester and W. A. Ferrando, Nucl. Instrum. and Methods 108, 599 (1973).
[38]R. L. Cohen and H. J. Guggenheim, Nucl. Instrum and Methods 71, 27 (1969).
[39]R. S. Feigelson, J. Am. Ceram. Soc. 47, 257 (1964).
[40]B. Khurgin, S. Ofer, and M. Rakavy, Phys. Lett. A 33, 219 (1970).
[41]W. Ebenhöh, V. J. Ehlers, and J. Ferch, Z. Phys. 200, 84 (1967).
[42]Shun-ichi Kobayashi, Naokatsu Sano, and Junkichi Itoh, J. Phys. Soc. Jpn. 21, 1456 (1966).
[43]R. Orbach, Proc. Phys. Soc. Lond. 77, 821 (1961).
[44]V. D. Gorobchenko, I. I. Lukashevich, V. G. Stankevich, E. V. Mel'nikov, and N. I. Filippov, Fiz. Tverd. Tela 14, 2468 (1972) [Sov. Phys.–Solid State 14, 2140 (1973)].
[45]R. P. Gupta and S. K. Sen, Phys. Rev. A 7, 850 (1973).
[46]B. Bleaney, in *Proceedings of the Third International Symposium on Quantum Electron, Paris* (Columbia U. P., New York, 1964), p. 595.
[47]H. H. Wickman and I. Nowik, Phys. Rev. 142, 115 (1966).
[48]B. Elbeck, K. O. Nielsen, and M. C. Olesen, Phys. Rev. 108, 406 (1957).
[49]O. V. Lounasmaa, in *Hyperfine Interactions*, edited by A. J. Freeman and R. B. Frankel. (Academic, New York, 1967) Chap. X.